J Mater Sci (2007) 42:3307–3314
DOI 10.1007/s10853-006-0570-1

SIZE-DEPENDENT EFFECTS

Effects of morphology and cesium promotion over silver nanoparticles catalysts in the styrene epoxidation

Ricardo José Chimentao · Francesc Medina · Jesús Eduardo Sueiras · José Luís García Fierro · Yolanda Cesteros · Pilar Salagre

Received: 10 May 2006 / Accepted: 14 June 2006 / Published online: 27 February 2007

Abstract Silver nanowires have been obtained by polyol reduction of silver nitrate in presence of polyvinyl-pyrrolidone (PVP). The as-synthesized silver nanowires were deposited on α- Al_2O_3. For comparison silver catalysts were also prepared by wetness impregnation obtaining irregularly shaped silver particles. Epoxidation of styrene to styrene oxide (SO) by molecular oxygen was studied using the silver catalysts. The main products were styrene oxide (SO) and phenylacetaldehyde (Phe). The promotion effect of the Cs on the silver nanowires catalysts was investigated. The Cs loading was in the range of 0–1 wt.% (refereed to silver). Furthermore, the effect of O_2:C_8H_8 molar ratio on the catalytic epoxidation was also investigated. Silver nanowires catalysts showed superior catalytic activity compared to those prepared by impregnation method. Besides, higher O_2:C_8H_8 ratios improved the selectivity to SO. The catalytic activity showed a maximum performance for silver nanowires promoted with 0.25 wt.% of Cs, achieving 94.6% of conversion and total selectivity to desired oxidation products (styrene oxide and phenylacetaldehyde). Moreover, the cesium promotion also contributed to the increase in the selectivity to styrene oxide. Temperature programmed reduction (TPR) and X-ray photoelectron spectroscopy (XPS) were employed to detect the presence of different species of oxygen in the catalysts indicating that subsurface oxygen was beneficial for the epoxidation. The samples were also structurally characterized using X-ray diffraction (XRD), scanning electron microscopy (SEM), transmission electron microscopy (TEM), UV-visible absorption spectra and selected area electron diffraction pattern (SAED).

R. J. Chimentao · F. Medina (✉) · J. E. Sueiras
Dept. d'Enginyeria Química, Universitat Rovira i Virgili, 43007 Tarragona, Spain
e-mail: fmedina@etse.urv.es

J. L. G. Fierro
Instituto de Catalisis y Petroleoquimica, CSIC, 28049 Cantoblanco, Madrid, Spain

Y. Cesteros · P. Salagre
Dept. de Química Inorgánica, Universitat Rovira i Virgili, 43007 Tarragona, Spain

Introduction

Materials in nanometer scale are of great interest due to their unique optical, electrical, and magnetic properties. These properties are strongly dependent on the size and the shape of the particles and therefore it is very important to be able to finely control the morphology of the nanomaterials [1, 2]. Besides, these materials have a large fraction of surface atoms per unit of volume [3]. The ratio of surface atoms to bulk depends on the particle size. So, a dramatic increase in this ratio can be expected for metal nanoparticles changing the physical and chemical properties of these materials [4]. Current research has been focused on one-dimensional nanoparticles such as nanorods and nanowires since the morphological anisotropy results in very complex physical properties and self assembly behaviors compared to those bulk materials [5]. Metal particles have been synthesized by using various methods such as templating [6, 7], photochemistry [8], seeding [9, 10], and electrochemistry [11, 12]. Reduction of the metal complexes in diluted solutions is the

general method in the synthesis of metal nanoparticles. The formation of monosized metallic nanoparticles can be achieved in most cases by a combination of a low concentration of solute and the use of polymeric stabilizers such as polyvinyl-pyrrolidone (PVP). Silver nanowires have been synthesized via polyol process [13]. Ethylene glycol has been widely used in this synthesis process due to its strong reducing power and relatively high boiling point [14]. The growth of the Ag particles is generated by the reduction of $AgNO_3$ with ethylene glycol whereas the anisotropy growth is controlled by the presence of stabilizers such as PVP.

The control of the dimensions and morphology of silver nanoparticles could be of great interest to obtain more active and selective catalysts. In this sense, it has been observed that metal nanoparticles have a superior catalytic behavior [15]. In this account, we report the synthesis of shape controlled silver nanoparticles and the application of the resultant materials in the study of the epoxidation of styrene in gas phase using molecular oxygen as oxidant. Styrene ($C_6H_5CH = CH_2$) is a good choice because the phenyl group π-electrons activate the olefinic bound towards electrophilic attack by oxygen [16]. Epoxides are industrially important bulk chemicals. These compounds are largely used for synthesis of several perfumes, epoxy resins, plasticizers and drugs. Therefore the synthesis of epoxides is of great interest. Unfortunately, due to the reactivity of epoxides, they are often difficult to prepare with high selectivity and high yields. Ethylene is the only olefin that has been successfully oxidized employing molecular oxygen on a commercial scale to produce the epoxide. Silver is considered almost the unique effective catalyst for ethylene epoxidation [17] and α-Al_2O_3 is the preferred support. Besides, alkali metals and their salts have been proposed as promoters for these catalysts [18]. In this sense, we also investigated the addition of cesium in the catalytic activity of the silver nanowires. Besides, the effect of the O_2: styrene molar ratios in the catalytic behavior were also studied. For comparison a catalyst prepared by wetness impregnation with an aqueous solution of $AgNO_3$ was also performed.

Temperature programmed reduction (TPR) and X-ray photoelectron spectroscopy (XPS) were performed to characterize the oxygen species formed on the silver nanowires after exposure to O_2. The samples were also structurally characterized using X-ray diffraction (XRD), scanning electron microscopy (SEM), transmission electron microscopy (TEM), UV-visible absorption spectra and selected area electron diffraction pattern (SAED) in order to correlate the morphological dependence of metal particles with the catalytic behavior.

Experimental

Catalyst preparation

The support used was α-Al_2O_3 (Degussa, Type 221) with a grain size of 45–175 μm and a specific surface area (S_{BET}) of 0.4 $m^2\ g^{-1}$. The as-received support was calcined in static air at 800 K for 4 h before metal incorporation. The catalysts were prepared by two procedures. First, wetness impregnation method was used to impregnate α-Al_2O_3 support with an appropriate amount of an aqueous solution of silver nitrate to obtain 11 wt% of silver. In the second procedure, silver nanoparticles were synthesized via polyol process. In a typical synthesis of silver nanoparticles, 30 mL of ethylene glycol solution of $AgNO_3$ (0.25 M, Aldrich) and 30 mL ethylene glycol solution of PVP (0.375 M in repeating unit weight-average molecular weight ≈ 40000, Aldrich) were simultaneously added in 50 mL ethylene glycol at 433 K under vigorous stirring. The reaction mixture was then refluxed for 45 minutes at this temperature. The nanoparticles obtained were diluted with acetone (about 10 times by volume) and separated from ethylene glycol by centrifugation at 4000 rpm for 20 minutes. Silver nanowires (11%wt.) were dispersed on α-Al_2O_3 with an acetone solution. Finally, silver nanowires catalysts were dried in an oven at 393 K for 24 h and reduced in H_2 at 623 K for 3 h before the characterization and the activity tests. To investigate the promotion effect of cesium, silver nanowires catalysts were impregnated by an aqueous solution containing appropriate amounts of CsOH. The catalysts were prepared with different Cs loading (0.0625, 0.125, 0.25, 0.5 and 1 wt.%). After that the promoted catalyst was activated using the same protocol.

Catalyst characterization

The metal content in the samples was determined by ICP-AES (Philips Scientific PU 7000 spectrometer). X-ray diffraction (XRD) measurements were made using a Siemens D5000 diffractometer (Bragg–Bentano parafocusing geometry and vertical θ–θ goniometer) fitted with a grazing incident (ω: 0.52°) attachment for thin film analysis and scintillation counter as a detector. The samples were dispersed on Si (510) sample holder. The angular 2θ diffraction range was between

10° and 120°. The data were collected with an angular step of 0.03° at 12 s per step and sample rotation. $Cu_{K\alpha}$ radiation (λ = 1.54056 Å) was obtained from a copper X-ray tube operated at 40 kV and 30 mA. The crystalline phases were identified using the JCPDS files. The morphologies of the catalysts were observed by SEM with a JEOL JSM-35C scanning microscope operated at an acceleration voltage of 15 kV. Further structural analyzes were performed by TEM in a JEOL JEM-2000EX II microscope operated at 80 kV. The solid sample, which was homogeneously dispersed in pure acetone by means of an ultrasonic bath, was deposited in the copper grid and then the solvent was evaporated under vacuum before TEM analysis.

Temperature programmed reduction was performed using a Thermo Finnigan instrument TPD/R/O/1100, equipped with a thermal conductivity detector (TCD) and coupled to a mass spectrometer QMS 422 Omnistar. The sample (40 mg) was first pretreated in a quartz reactor with a gas flow containing O_2 and N_2 at 673 K for 1 h followed by purging with high purity argon. After the sample was cooled to 323 K, an H_2–Ar (5 vol% H_2) mixture was introduced into the reactor and the temperature was raised to 1073 K at a rate of 10 K min^{-1} at a flow of 20 mL/min.

The XPS spectra were acquired in a VG Escalab 200R electron spectrometer equipped with a hemispherical electron analyzer, operating in a constant pass energy mode, and a non-monochromatic Mg–Kα (hv = 1253.6 eV, 1 eV = 1.603×10^{-19} J). X-ray source operated at 10 mA and 12 kV. The background pressure in the analysis chamber was kept below 7×10^{-9} mbar during data acquisition. The binding energy (BE C1s = 284.9 eV) of adventitious C_1 was used as reference. A Shirley background subtraction was applied and Gaussian-Lorentzian product functions were used to approximate the line shapes of the fitting components.

The gas-phase epoxidation of styrene was studied in a fixed-bed tubular stainless steel reactor (10 mm i.d.) between 503 and 523 K using 1.0 g of catalyst. The reaction temperature was controlled by a thermocouple located inside the catalytic bed. A mixture of O_2–Ar was fed to the reactor by independent mass flow controllers, using a total flow rate between 100–300 mL/min. The styrene was introduced into the reactor by a high-pressure metering pump in a flow-rate range of 0.08–0.5 mL/h. The reaction products were analyzed on-line using a Shimadzu GC 2010 gas-chromatograph equipped with an Ultra 2 capillary column and a flame ionization detector (FID). The presence of combustion products was determined by on-line TCD and mass spectrometer.

Results and discussion

On the basis of the reaction of silver nitrate and PVP in EG at 433 K, once the solutions of $AgNO_3$ and PVP had been introduced to the reaction system, a bright yellow color gradually appeared indicating the formation of silver nanoparticles through the reduction of $AgNO_3$ with ethylene glycol. Figure 1(a) shows the XRD pattern for the sample taken from the yellow solution corresponding to 15 min of polyol process and Fig. 1(b), the respective TEM image. One broad diffraction line corresponding to the (111) lattice plane was detected by XRD for silver nanoparticles. By TEM was observed that the main size for these silver nanoparticles was around 5 nm. The selected-area diffraction pattern (SAED) taken from these Ag nanoparticles exhibited Debye-Scherrer rings (inset Fig. 1b) which are assigned to (111), (200) and (220) reflections of the face centered cubic structure (fcc) of silver. The surface analysis of these silver nanoparticles was evaluated by X-ray photoelectron spectroscopy (XPS). The corresponding XPS core-level spectra of the Ag-3*d* region acquired for these silver nanoparticles sample is depicted in Fig. 2. The Ag-3*d* spectra, characterized by the spin-orbit splitting (Ag $3d_{5/2}$ and Ag $3d_{3/2}$ components), shows values off 367.97 and 374.18 eV, respectively. Both peaks indicate that these binding energies are consistent with Ag^0 oxidation state [19, 20].

During polyol process, the mixture solution changed from clear to a yellowish color, red brown and finally to gray. Figure 3(a, b) shows UV-vis spectra as well as the resultant colors of the samples during the synthesis of silver nanoparticles by polyol process. The growth of silver nanowires was monitored by sampling aliquots from the refluxing solution at different periods of time and analyzing these samples by ultraviolet visible spectroscopy (UV-vis). The spectrum of the solution at 15 min (yellow solution) shows a small plasmon band close to 410 nm, which represents the formation of silver nanoparticles by the reduction of Ag^+ ions [21]. The appearance of the plasmon band is caused by 4d $\rightarrow$ 5s, p interband transitions [22]. The intensity of this band progressively increased during polyol process. Besides, the absorption band of the silver nanoparticles is shifted to larger wavelengths with the refluxing time. The nanoparticles obtained at 40 min (gray solution) displayed a broad peak at around 430 nm. The gray solution is formed by predominantly silver nanowires particles.

The X-ray diffraction of these silver nanowires suggested that silver existed purely in the face-centered cubic (fcc) structure (Fig. 4). The presence of possible

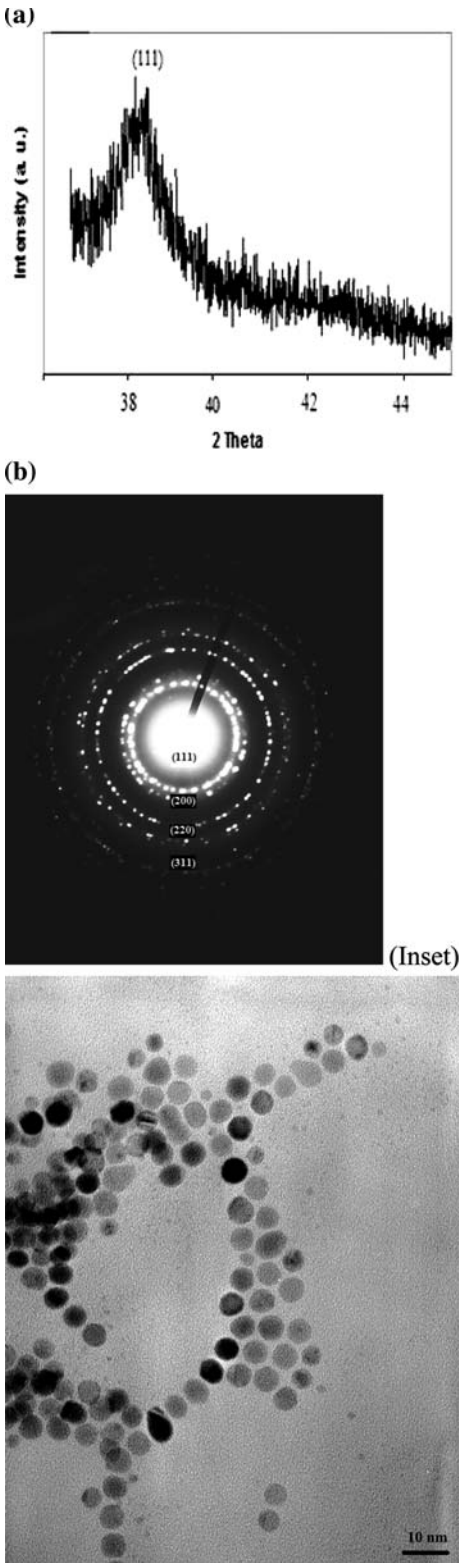

Fig. 1 (**a**) XRD of the sample taken from the polyol process during the first 15 min of the synthesis. (**b**) TEM image of the silver nanoparticles in the first 15 min of the polyol process. Inset: The selected-area diffraction pattern (SAED) taken from these Ag nanoparticles

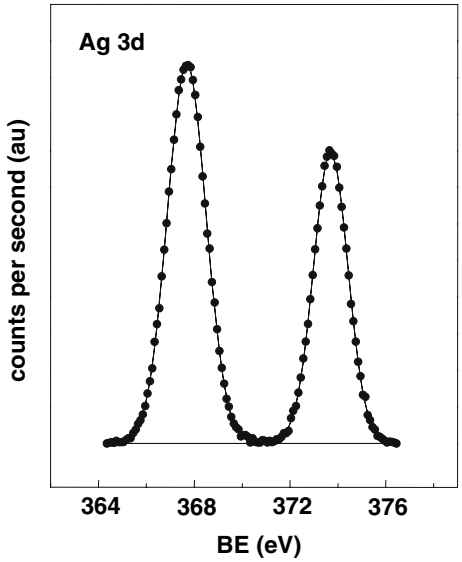

Fig. 2 Corresponding XPS analysis of the silver nanoparticles taken in the first 15 min of the polyol process

impurities such as Ag_2O and $AgNO_3$, was not detected. The lattice constants calculated by XRD for the nanowires was 4.0839, which is very close to the report data (a = 4.0862 Å, Joint Committee on Powder Diffraction Standards file 04-0783). The ratio of intensity between (111) and (200) peaks for nanowires was 4.5, that is higher than for the standard file (JCPDS) (4.5 vs. 2.5). This indicates that nanowires show preferred orientation in (111) facets. In order to elucidate the structure of the Ag nanowires, a drop of the silver nanowires EG colloidal solution was analyzed by scanning electron microscopy. The SEM image (Fig. 5a) shows that monodispersed nanowires were obtained. The average diameter for silver nanowires was around 150 nm. However, together with the silver nanowires (but in low amount) the presence of nanocubes and nanopolyhedra were also observed. The cross section of the silver nanowires in the SEM image (Inset of Fig. 5a) clearly shows a pentagonal shape in agreement with previous results [23]. In general, silver single crystal has a face-centered cubic (fcc) structure, therefore the pentagonal shape of the cross-sections indicates the multiple—twinned structure of the Ag nanowires. Nanowires tend to grow as bicrystals twinned along the (111) planes, showing (111) crystal faces at their surface [24].

Silver nanowires catalysts were prepared by impregnation of α-Al_2O_3 support with an acetone solution of silver nanowires. The amount of silver was 11 wt.% obtaining the catalyst labeled as $11\%Ag^{(NW)}/\alpha$-Al_2O_3. A silver impregnated catalyst ($11\%Ag/\alpha$-Al_2O_3) was also prepared for comparison. SEM image

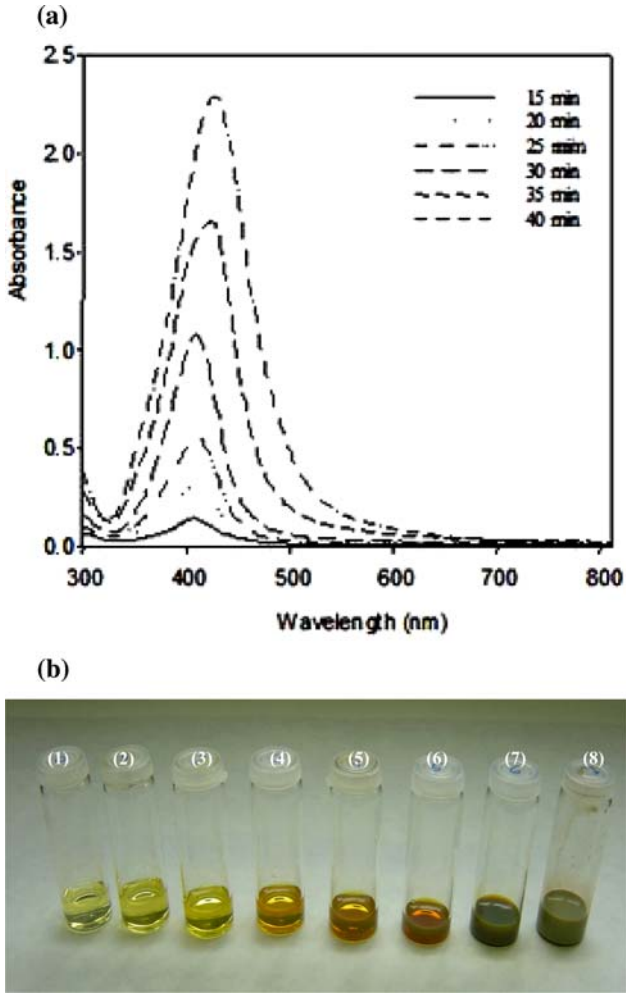

Fig. 3 UV-vis spectra during the formation of silver nanowires (**a**). Picture of the samples (1–8) taken from reaction mixture during different periods of time in the polyol process (**b**)

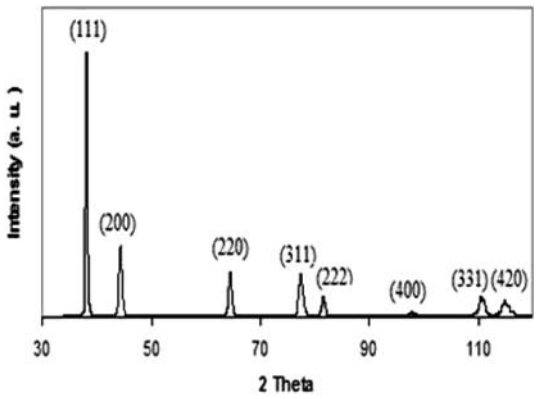

Fig. 4 XRD pattern of the silver nanowires obtained by the polyol process

of this catalyst is shown in Fig. 5b, showing irregular shape particles.

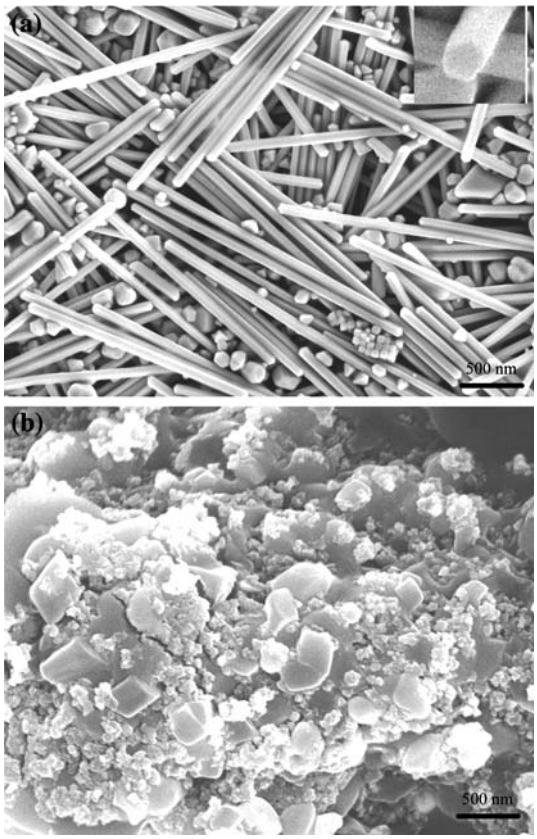

Fig. 5 SEM image of the as-prepared silver nanowires by the polyol process (**a**) and silver impregnated catalyst (**b**)

The reducibility of silver catalysts as well as the effect of the addition of cesium was studied by TPR (Fig. 6). Two oxygen peaks were observed over silver catalysts. The unpromoted silver nanowires catalyst (Inset Fig. 6,(a)) shows two broad peaks at around 633 K (the most intense peak) and 873 K. Previous studies of oxygen adsorption on silver have attempted to characterize the nature of adsorbed species. The peak around 600 K has been attributed to the presence of subsurface oxygen (O_β) [25–31]. The presence of reduction peaks at higher temperatures can be attributed to the presence of oxygen species that are strongly chemisorbed on the surface of silver and are labeled as (O_γ) [28, 32–34]. For the impregnated catalyst (Inset Fig. 6, (b)) the reduction peaks were shifted to higher temperatures (753 K and 933 K, respectively). The most intense peak for this catalyst was the second one. The influence of the addition of cesium on the reducibility of silver nanowires catalyst ($11\%Ag^{(NW)}/\alpha\text{-}Al_2O_3$) is illustrated in Fig. 6 and Table 1. Practically one main peak is observed for cesium promoted silver nanowires catalysts. The addition of cesium increases the peak signal and reduces also the temperature of reduction when compare with unpromoted silver

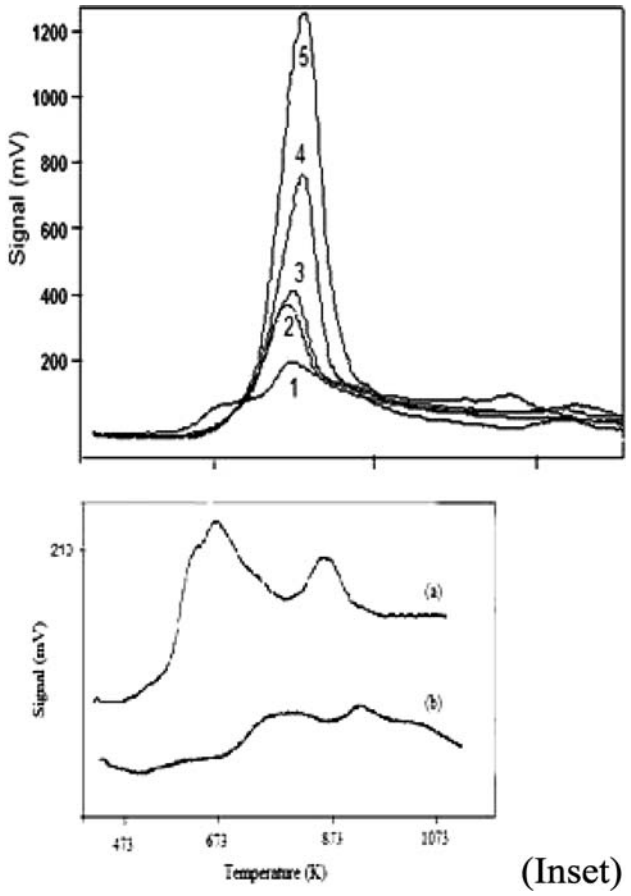

Fig. 6 Temperature programmed reduction profiles (TPR) of various loading of cesium (refereed with the silver content) on $11\%Ag^{(NW)}/\alpha\text{-}Al_2O_3$ catalyst. (1) 0.0625%, (2) 0.125%, (3) 0.25%, (4) 0.5%, (5) 1.0%. Inset: unpromoted silver nanowires (**a**) and impregnated silver catalyst (**b**)

nanowires catalyst. This peak can be attributed to O_β species.

The XPS data was also consistent with the TPR results. From Fig. 7, the O1s peak signal observed for the unpromoted silver nanowires was around 529.7 eV. However, when cesium was added the O1s peak showed two components, the major one at around 531.5 eV and a less intense one at around 529.8 eV. The deconvoluted peak of the O1s component with a binding energy value of around 531.5 eV represents around 90% for the sample oxidized at 623 K These O-species have been ascribed to O_β (531.5 eV) and O_γ species (529.8 eV) [26, 32]. From the XPS results it can be concluded that O_γ was the unique specie detected for the unpromoted silver nanowires while O_β was the major oxygen species detected by XPS for cesium promoted samples.

Table 1 shows the catalytic performance of the silver catalysts for the epoxidation of styrene with molecular oxygen as oxidant. A blank test run with the $\alpha\text{-}Al_2O_3$ support showed no conversion of styrene at the reaction temperature studied (523 K). It is important to mention that the deactivation of the catalyst during the operation time (around 30 days) was negligible. The impregnated catalyst showed a styrene conversion of 1% at this reaction temperature. However, for silver nanowires catalyst a conversion of 10% was observed at the same reaction conditions. It is of interest to note that the presence of the alkali metal not only enhances the selectivity to SO but also increase the styrene conversion. The addition of cesium in silver nanowires catalysts increased the catalytic activity. The highest activity (94.6% of conversion) was observed for a cesium loading of 0.25 wt.%. Beyond this limit the activity decreased progressively. The selectivity to styrene oxide increased from 42.5% for unpromoted catalyst up to 75.9% when silver nanowires catalyst was promoted with 1 wt.% of cesium. The decrease of conversion at higher Cs loadings (Cs > 0.25 wt.%) can be probably attributed to the effect of cesium dispersion. This fact was reinforced by the results obtained by XPS that are shown in Table 2. The sample with a cesium loading of 0.125 wt.% shows a Cs/Ag atomic ratio of 0.119. When the cesium increased up to 0.25 wt.% the Cs/Ag ratio increased up to 0.24. However for samples with higher cesium content the Cs/Ag atomic ratios decreased. For instance, the 11% $Ag^{(NW-1.0\%Cs)}/\alpha\text{-}Al_2O_3$ sample, which has four times of cesium amount than for $11\%Ag^{(NW-0.25\%Cs)}/\alpha\text{-}Al_2O_3$, the Cs/Ag molar ratio detected by XPS analysis is quite similar (around 0.2). This fact may indicates that agglomeration of cesium species is produced at higher cesium loading, that may cover the silver surface inducing the poisoning of the active sites.

Table 1 Results of temperature- programmed reduction and catalytic activity tests for the $11\%Ag^{(NW)}/\alpha\text{-}Al_2O_3$ catalyst unpromoted and promoted at 523 K

Catalyst	TPR analysis	Catalytic activity		
	T_{max} (K)[a]	X (%)[b]	Phe (%)[c]	SO (%)[d]
$11\%Ag/\alpha\text{-}Al_2O_3$	753	1.00	51.4	48.6
$11\%Ag^{(NW)}/\alpha\text{-}Al_2O_3$	623	10.0	57.5	42.5
$11\%Ag^{(NW\text{-}0.0625\%Cs)}/\alpha\text{-}Al_2O_3$	568	50.9	48.6	51.4
$11\%Ag^{(NW\text{-}0.0125\%Cs)}/\alpha\text{-}Al_2O_3$	570	60.1	46.8	53.2
$11\%Ag^{(NW\text{-}0.25\%Cs)}/\alpha\text{-}Al_2O_3$	572	94.6	44.4	55.6
$11\%Ag^{(NW\text{-}0.5\%Cs)}/\alpha\text{-}Al_2O_3$	583	72.4	25.1	74.9
$11\%Ag^{(NW\text{-}1.0\%Cs)}/\alpha\text{-}Al_2O_3$	587	42.3	24.1	75.9

[a] Peak signal from the first peak detected by temperature programmed reduction (TPR)

[b] Conversion (X)

[c] Selectivity to phenylacetaldehyde (Phe%)

[d] Selectivity to styrene oxide (SO%), O_2: C_8H_8 molar ratio of 50

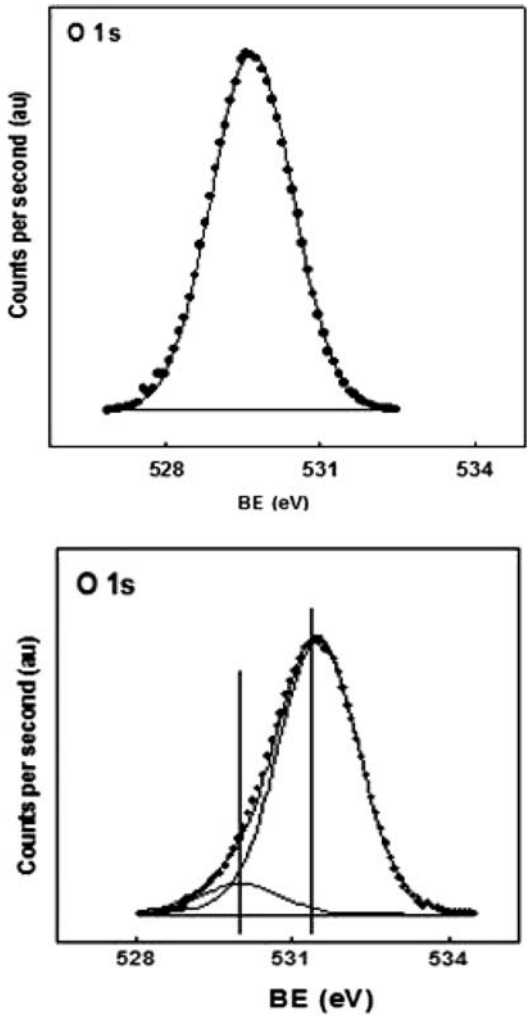

Fig. 7 In situ XPS profiles of the silver nanowires unpromoted and promoted by 0.25% of Cs after oxidation at 623 K

Table 3 lists the conversion and selectivity for styrene epoxidation reaction on 0.25 wt.% cesium promoted silver nanowires at 503 K and different C_8H_8: O_2 molar ratios. The increase in the O_2: C_8H_8 molar ratio also improved the conversion and selectivity to styrene oxide. When the O_2: C_8H_8 molar ratio was 25, the conversion was 59.3% and the selectivity reaches 55.3%, while for O_2: C_8H_8 molar ratio of 150 the conversion was 84.2% and the selectivity to styrene oxide was 73.5%. It seems that an oxygen rich atmosphere is also beneficial for the epoxidation of styrene. These results are in agreement with previous work that indicated similar trends [35].

Table 2 ICP-AES and XPS surface analysis of the silver nanowires catalyst

Catalyst	ICP-AES analysis (Atomic ratio)		XPS analysis (Atomic ratio)	
	Cs/Al	Cs/Ag	Cs/Al	Cs/Ag
$11\%Ag^{(NW\text{-}0.125\%Cs)}/\alpha\text{-}Al_2O_3$	0.00005	0.0009	0.005	0.119
$11\%Ag^{(NW\text{-}0.25\%Cs)}/\alpha\text{-}Al_2O_3$	0.0001	0.0018	0.009	0.240
$11\%Ag^{(NW\text{-}0.5\%Cs)}/\alpha\text{-}Al_2O_3$	0.0002	0.0036	0.020	0.119
$11\%Ag^{(NW\text{-}1.0\%Cs)}/\alpha\text{-}Al_2O_3$	0.0004	0.0072	0.023	0.220

Table 3 The conversion and selectivity of styrene epoxidation on $11\%Ag^{(NW\text{-}0.25\%Cs)}/\alpha\text{-}Al_2O_3$ catalyst[a]

Ratio molar O_2:C_8H_8	Conversion (%)	Selectivity to SO (%)
25	59.3	55.3
50	76.5	68.4
100	79.7	70.5
150	84.2	73.5

[a] Reaction temperature: 503 K

Conclusion

Ag nanowires have been prepared by polyol process using PVP as a structure-directing agent. Styrene epoxidation by oxygen was carried out on silver nanowires promoted with different contents of cesium. The addition of cesium improves the catalytic activity. The maximum activity was obtained when the silver nanowires were promoted by 0.25% of Cs. In addition the selectivity to styrene oxide also increased with the addition of cesium. Phenylacetaldehyde and styrene oxide were the main products under our reaction conditions. The impregnated catalyst (11% Ag/α-Al_2O_3) showed the lowest catalytic activity performance. Besides, a rich oxygen atmosphere was beneficial to the catalytic performance. It is also important to note that the deactivation of the catalysts was negligible even after 30 days of operation. Catalyst preparation method and reaction conditions have a strong influence both in activity and selectivity toward desired products. The shape control of silver nanoparticles seems to have potential catalytic applications in the study of the selective oxidation of olefins.

Acknowledgements This work was supported by the Ministerio de Ciencia y Tecnologia (Spain) under Projects REN2002-04464-CO2-01 and PETRI 95-0801.OP.

References

1. Creighton JA, Eadon DG (1991) J Chem Soc Faraday Trans 87:3881
2. Cao Y, Jin R, Mirkin CA (2001) J Am Chem Soc 123:7961

3. Nutzenadel C, Zutell A, Chartouni D, Shimid G, and Schalapbach L (2000) Eur Phys J D8 245
4. Kim F, Kwan S, Akana J, Yang P (2001) J Am Chem Soc 123:4360
5. Goldstein AN, Echer CM, Alivisatos AP (1992) Science 256:1425
6. Bohmer MR, Fokkink LGJ, Schonenberger C, Van Der Zande BMI (1997) J Phys Chem B 101:852
7. Nicewarner SR, Freeman RG, Reiss BD, He L, Pena DJ, Walton ID, Cromer R, Keating CD, Natan MJ (2001) Science 294:137
8. Esumi K, Matsuhisa K, Torigoe K (1995) Langmuir 11:3285
9. Murphy CJ, Jana NR (2002) Adv Mater 14:80
10. Sun YG, Xia YN (2002) Adv Mater 14:833
11. Yu YY, Chang SS, Lee CL, Wang CRC (1997) J Phys Chem B 101:6661
12. Chang SS, Shih CW, Chen CD, Lai WC, Wang CRC (1999) Langmuir 15:701
13. Wang ZL, Mohamed MB, Link S, El-Sayed MA (1999) Surf Sci 440:L809
14. Sun Y, Xia Y (2002) Science 298:2176
15. Sun Y, Gates B, Xia Y (2002) Nano Lett 2:165
16. Williams FJ, Bird DPC, Sykes ECH, Santra AK, Lambert RM (2003) J Phys Chem B 107:3824
17. Campbell CT (1985) J Phys Chem 89:5789
18. Sachtler WMH, Backx C, Van Santen RA (1981) Cat Rev Sci Eng 23:127
19. Scofield JH (1976) J Electr Rel Phen 8:129
20. XPS International fundamental XPS data tables, www. xps-data.com
21. Han HJ, Koo SM (2003) J Sol-Gel Sci Tech 26:467
22. Meisel D (1998) J Phys Chem B 102:8364
23. Murphy CJ, Jana NR (2002) Adv Mater 14:80
24. Cullity BD, Stock SR (2001) Elements of X-ray diffraction, 3rd edn. Prentice-Hall, Upper Saddle River, N.J., pp 402–404
25. Nagy AJ, Mestl G, Herein D, Weinberg G, Kiltzelmann E, Schlogl R (1999) J Catal 182:417
26. Nagy AJ, Mestl G (1999) Appl Catal 188:337
27. Nagy AJ, Mestl G, Schlogl R (1998) J Catal 188:58
28. Herein D, Nagy A, Schubert H, Weinberg G, Kitzelmann E, Schlogl R (1996) Z Phys Chem 197:67
29. Nagy AJ, Mestl G, Herein D, Weinberg G, Kiltzelmann E, Schlogl R (1999) J Catal 182:417
30. Somorjai GA (1994) Introduction to surface chemistry and catalysis. Wiley, New York
31. Li WX, Stampfl CS, Scheffler M (2003) Phys Rev B 67:045408
32. Bao X, Muhler M, Scedel-Niedrig T, Schlogl R (1996) Phys Rev B 54:2249
33. Nagy A, Mestl G, Rule T, Weinberg G, Schogl R (1998) J Catal 179:548
34. Waterhouse GIN, Bowmaker GA, Metson JB (2003) Appl Catal 214:36
35. Van Santen RA, Kuipers HPCE (1987) Adv Catal 35:265